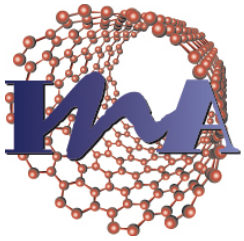

Instituto Universitario de Investigación
en Nanociencia de Aragón
Universidad Zaragoza

Master in physics and physical technologies

Master Thesis

Remote drug release study using ferrogels under AC fields

Ignacio J. Bruvera
Supervisor: Dr.Gerardo F. Goya Rosetti

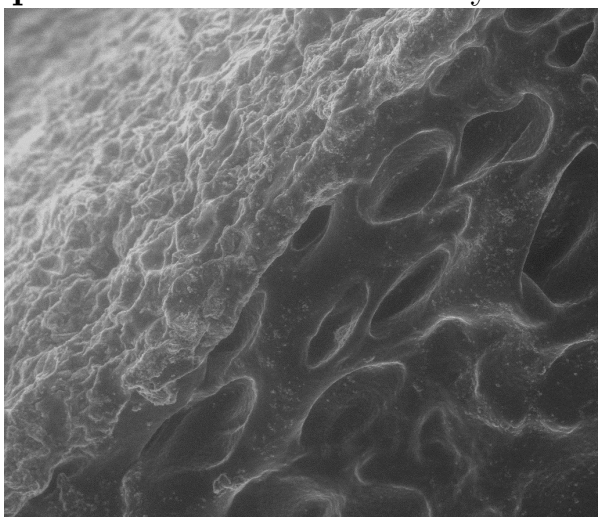

24 June 2012

Contents

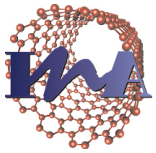

Instituto Universitario de Investigación
en Nanociencia de Aragón
Universidad Zaragoza

Remote drug release study using ferrogels under AC fields

Ignacio Javier Bruvera

E-mail: bruvera@unizar.es

Director:Gerardo F. Goya Rossetti

Instituto de Nanociencia de Aragón (INA). Universidad de Zaragoza Ed. I+D - Calle Mariano Esquillor s/n Campus Rio Ebro 50018-Zaragoza
Phone: (34) 976 76 2777 (ext 2987)
Fax: (34) 976 76 2776
web: http://www.unizar.es/gfgoya

Abstract. A dedicated device was built with the purpose of studing the remotely controlled drug release of a temperature sensitive hydrogel in a water flow. Samples of the hydrogel (semi-interpenetrating polymer networks constituted by alginate and PNIPAAm) with *in situ* synthesized magnetite nanoparticles (average size 10nm) were characterised by TEM, STEM/EDS, SEM, VSM and power dissipation measurements. These results were used to design and construct a system able to measure the drug release of the samples in a water flow when exposed to an external RF field. The device was calibrated to obtain absolute values of drug concentration in the water flow in real time by a built-in photometer. Vitamin B12 was used as model drug. First results indicate a good response of both the sample and the device. Field induced drug liberation events were clearly recorded. A liberated B12 mass in the order of 10ng was calculated for each event. Further experiments are necessary for a complete characterization of the drug release process.

1. Introduction

1.1. Magnetic nanoparticles

Magnetic nanoparticles (MNP) represent a very interesting field of study, both in the basic research as in applied science. In particular, its uses in biomedicine are numerous and with a intense development in the past decade [1].
One of the most commonly exploited characteristic of the MNP is its capacity of

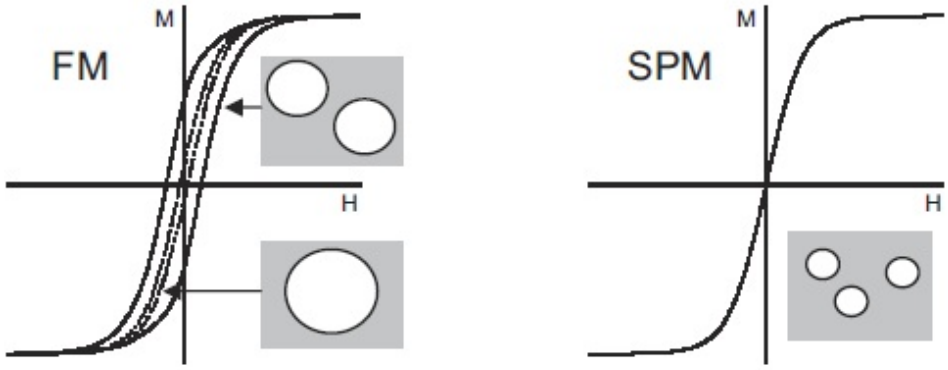

Figure 1. Basic shape of the Magnetization vs. Field plots for ferromagnetic (FM) big and small particles and superparamagnetic (SPM) particles (from [2]).

absorbing power from an AC electromagnetic field and then release it in the surrounding medium as heat. An important application of this phenomena is the Magnetic Fluid Hyperthermia (MFH) therapy used in cancer therapy. This technique consists in the injection of a suspension of MNP, called ferrofluid (FF), in the body of the patient and the exposure of the affected region to a AC field in order to increase its temperature. Tumour cells, more sensitive to high temperatures than healthy ones, then decrease their viability[3]. The MNP can be functionalized to interact preferentially with tumour cells and concentrate in the affected zone [6][7].

The size of the MNP is determinant for its magnetic response. Particles above $1\mu m$ are multidomain, they contain multiple regions of coordinated magnetic alignment separated by domain walls which require some energy to be moved. When a external field is applied, the domains with a magnetization parallel to the field direction grow at the expense of the rest. This can be seen in a magnetization vs. field measurement as a narrow hysteresis loop compared with the response of a bulk sample of the same material which has bigger domain walls. For smaller particles, the domain walls turn too expensive in energy since the surface to volume ratio increases. So they present a single domain state with a wider hysteresis loop since the whole particle must change its magnetization during the process. In particles under $100\mu m$ size, the magnetic moment is free to fluctuate due to thermal agitation and the remanence of the system disappear. This is called superparamagnetism (SPM)[2](Fig. 1).

The field power to heat conversion occurs in the SPM particles by two principal mechanism. Due the interaction between the MNP magnetic moment and the external field, the MNP can change the direction of its total magnetization or, if is allowed, rotate to reach the minimum energy orientation. In the first case, called Néel relaxation, a uniaxial MNP dissipates power when crossing the potential barrier between its two easy magnetization directions. In the second case, called Brown relaxation, the dissipation occurs due the viscous interaction with the medium(Fig.2). When this mechanism compete the fastest prevails.

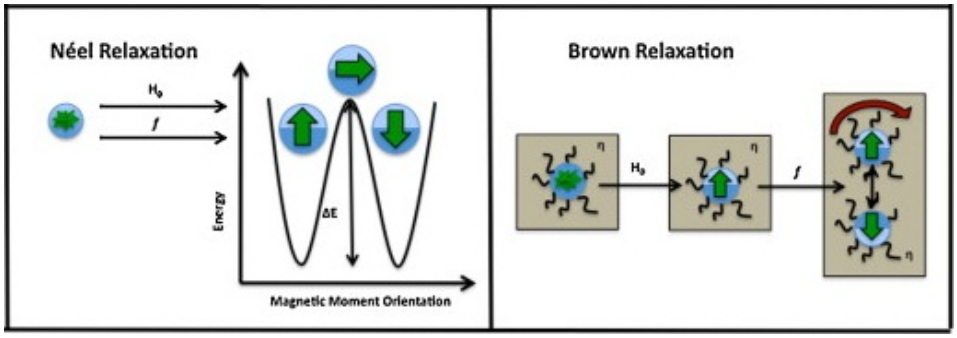

Figure 2. Schematic of the two relaxation mechanisms present when a FF of SPM particles is exposed to a RF field of amplitude H_c and frequency f . In Néel mechanism the magnetic moment orientation switches between the two easy axis jumping the anisotropy energy barrier ΔE. In Brown relaxation the MNP dissipate power when rotate in a medium with viscosity η [5].

1.2. Hydrogels

Hydrogels are crosslinked polymeric networks that absorb and retain large amounts of water[8]. The characteristic network structure of hydrogels is responsible for their unique ability to undergo abrupt volume changes in response to environmental stimuli such as change in pH, temperature or ionic strength[9].
It is known that the degree of swelling of gel is controlled by the free energy changes associated to both (i) the mixing of the polymer and water and (ii) the network elasticity. Related to that, there exist two general types of responsive microgels: (i) LCST-type (lower critical solution temperature) microgels such as the widely studied poly(N-isopropylacrylamide) and (ii) UCST-type (upper critical solution temperature) microgel such as poly(acrylamideacrylic acid) first reported by Bouillot and Vincent. Systems that show LCST-type volume phase transition temperature present a negative change of enthalpy and entropy. As the temperature increases, the entropic contribution to the energy grows leading to the phase separation and, thus, the shrinkage of microgel; therefore, LCST-type systems collapse upon heating. On the contrary, UCST-type microgel exhibits a positive swelling response related to the positive change of the enthalpy and entropy. The swelling behavior, and hence volume phase transition, is driven by hydrogen bonding that causes the microgel to shrink at temperatures below the UCST and swell at temperatures above the UCST[10].

1.3. Ferrogels:State of the Art

A method to obtain ferrogels with response to temperature and magnetic fields has been recently described. Iron oxide magnetic nanoparticles (MNP) synthesis is carried out through coprecipitation of iron salts in alkaline solutions inside semi-interpenetrating (semiIPN) polymer networks constituted of alginate and poly(N-isopropylacrylamide)(PNIPAAm)[11]. These ferrogels exhibit an improved deswelling rate with respect to pure PNIPAAm. In addition, the synthesis *in situ* of MNP inside

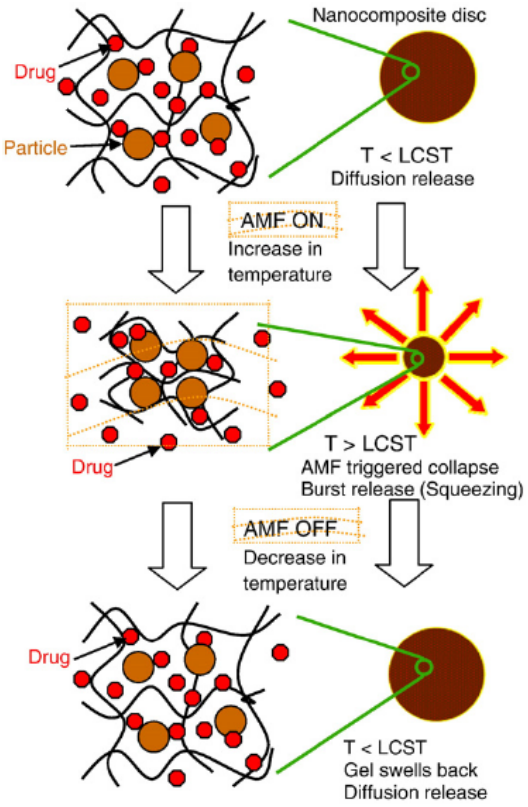

Figure 3. Schematic showing the effect of ONOFF cycles of a RF field on the magnetic nanocomposites of NIPAAm. It shows the field triggered collapse and resultant burst release due to squeezing effect.LCST=lower critical solution temperature [4]

.

Alg-PNIPAAm semi-IPNs allows controlling the polydispersity of the particles when compared to the reaction carried out in an alginate solution. The polymeric gel acts as a spatial framework to control the MNP size distribution [12]. Results on magnetic properties and heating experiments on hydrogels derived from polysaccharides (chitosan and alginate) have been reported showing good response to external radiofrequency (RF) magnetic fields, opening the possibility of using them as smart drug delivery materials for bioapplications[13].

The general motivation for this work is the study of magnetic hybrid poly(acrylamide-acrylic acid) thermoresponsive random copolymer hydrogel samples as a remote controlled drug release device. The hydrogel presents a tunable temperature triggered face transition that can be driven by an external RF field thanks to the MNP contained in the sample. In this way, a portion of gel hydrated in a water soluble drug solution can be use as a carrier and controlled releaser of this drug *in vivo*. (Fig.3)

Static release experiments have been made but not published yet by Hernández *et al*[14]. In this experiments, the liofilised hydrogel samples were first immersed in a PBS solution (12.5 g/l vitamin B12) for 48 h. The amount of B12 taken by the gel was determined by spectrophotometric measurements of small volumes of the solution:

a calibration was made first by measuring the absorbance at 361nm of B12 solutions of known concentration in a UV-Vis spectrophotometer. The samples from the gel bath were diluted and then measured in the same way.
For the release experiment the gels were transferred into 10 ml of PBS at 37^oC. Samples of 0.2 ml of the bath were taken at certain times and replaced by the same volume of PBS so that the total volume remained constant (10 ml). Each aliquot was diluted to 3 ml to measure absorbance at 361nm. The experiment was repeated with the PBS bath at 25^oC.
The comparison of the two experiments shows important differences between them: the hydrogel at 37^oC completely released the loaded vitamin B12 and the release occurs faster and in larger extension due to the collapse of the hydrogel. The natural next step in the direction of an *in vivo* application is the study of the dynamic release of the gel under a RF field in a water flow. With that propose, an *ad hoc* device must be constructed. This device must:

- Circulates a controlled water flow around the sample.
- Exposes the sample to a controlled RF field.
- Be adiabatic.
- Measures water and sample temperatures.
- Measures B12 concentration in the water flow in function of time.

2. Experimental

2.1. Sample synthesis

Semi-interpenetrating polymer networks constituted by alginate and PNIPAAm were obtained as reported elsewhere[11],[12]. The synthesis of iron oxide nanoparticles inside Alg-PNIPAAm semi-IPN hydrogels involves two steps. As a first step, gels are immersed in an acid solution containing Fe^{2+} and Fe^{3+}. As a second step, the gels are carefully immersed in an alkaline solution to oxidize the iron cations to iron oxide nanoparticles[13]. The mass of iron oxide nanoparticles in the ferrogels (WNP) was obtained from thermogravimetric analysis of dried ferrogels [11],[15]. The total water content, W_t, was calculated from the weight of the hydrated gels (M_s) and the weight of the dried gels (M_{dry}) as

$$W_t = M_{dry} - Ms/M_{dry} - M_{NP} \quad \text{(I)}$$

The samples were shaped as cylinders with 1cm diameter 4cm long and liofilized for a better manipulation.

2.2. Sample characterization

2.2.1. VSM : Small dry portions of the ferrogel (6.5(1)mg) and blank (14.2(1)mg) samples were measured in a Vibrating Sample Magnetometer (LakeShore 7304). A magnetization cycle in the range [-1.9,1.9]T was performed for each sample with a different point to point step for each field region ($B \in [0, 10]mT \rightarrow \Delta B = 0.5mT, B \in (10, 100]mT \rightarrow \Delta B = 10mT$ and $B \in (100, 1900]mT \rightarrow \Delta B = 100mT$).

2.2.2. SEM : Low vacuum SEM mesurements were performed in a environmental SEM-FEG (FEI Quanta 250). Ferrogel and blank samples in fully hydrated state were observed under different temperature/pressure/humidity conditions.

2.2.3. TEM : Conventional TEM images of dried ferrogel samples were taken by Hernández *et al* [13]. Additionally, samples were prepared by plunge-freezing in liquid ethane. Then, thin slices (less than 100nm) of the material were cut with the ultra-cryomicrotome, deposited on a copper grid and transferred under liquid nitrogen atmosphere (T=100K aprox.) to the TEM. The low temperature preserves the original state of the material; also, quick vitrification of the samples avoids the formation of crystalline ice, whose diffraction would interfere with the TEM observation.
Samples were then observed at liquid nitrogen temperature in a Tecnai T20 (FEI) equipped with a Lab6 filament and operated at 200KV. Bright field images were collected in a CCD camera with an acquisition time of 1s.
The same samples were also observed in a Tecnai F30 (FEI) equipped with a Field Emission Gun (FEG) operated at 300KV in Scanning Transmission (STEM) mode. A

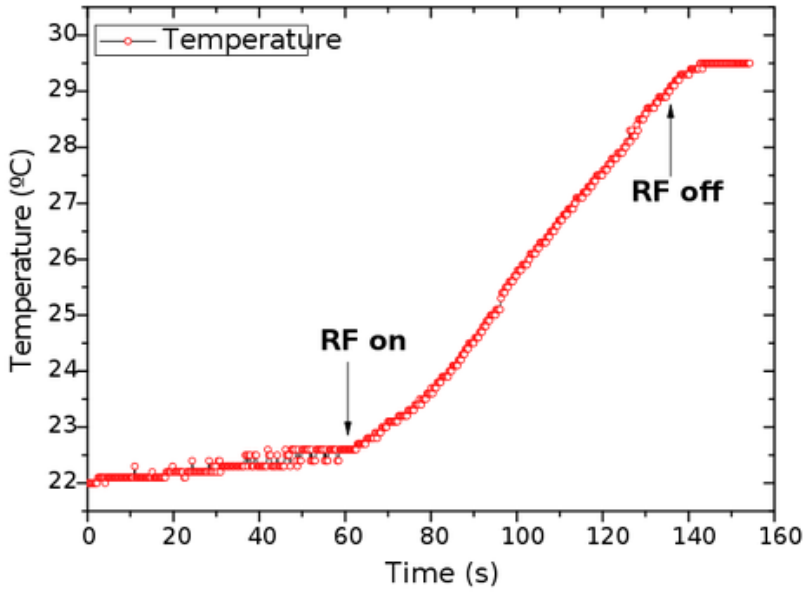

Figure 4. Heating curve of the hydrogel under RF field.t=0 in II indicates the moment of turning on the field.

narrow probe (1nm aprox in diameter) was formed and scanned over the surface of the sample. Thus, a High Angle Annular Dark Field (HAADF) image and a an Electron Dispersive X-Ray spectrum (EDS) were collected simultaneously for each pixel[17].

2.2.4. RF response : Power dissipation measurements were performed using a commercial AC applicator (EasyHeat)working at 360 kHz and field amplitudes up to 45kA/m equipped with an adiabatic sample space (∼0.5 ml) for measurements in liquid phase. Temperature data were taken using a fiber optic temperature probe (Reflex, Neoptix) immune to radio frequency environments. The power dissipated by the gel under the RF field P_{RF} is determined from the initial slope $\frac{\partial T}{\partial t}(0)$ of the T vs.t plot of the experiment (Fig.4) with the expression

$$P_{RF} = c_G m_G \frac{\partial T}{\partial t}(0) \qquad \text{(II)}$$

where c_G and m_G are the specific heat an mass of the gel sample.

2.2.5. Test drug. B12 vitamin: The test drug for the experiment must have two principal characteristics:

- Water solubility: the gel will be loaded with the drug by submerging it in an aqueous solution and will deswell in a water flow.
- Adequate optical activity: The determination of the drug concentration in the water flow will be made by spectrophotometric method. Therefore the test drug must have a well known absorption peak in an accessible wavelength range.
  There are more things to consider. The drug must be affordable since a big quantity

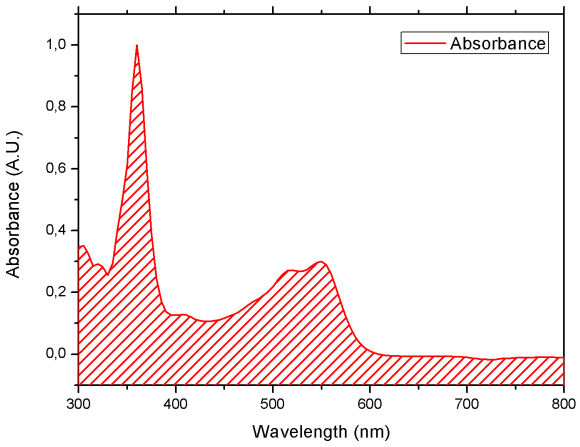

Figure 5. Absortion spectra of vitamin B12 in water in the UV-Vis range. Two well defined zones of maximum absorption can be seen: a sharp UV peak at 361nm and a wider region at [475, 575]nm.

will be used in the experiments and have to be safe to manipulate. With this considerations B12 vitamin (Sigma-Aldrich) was selected has drug model. The B12 is very soluble in water an has two well defined absorption peaks in the UV-Vis range (Fig.5).

2.3. Device design

The device consists of a water circuit propelled by a peristaltic pump. The circuit is composed by: a reservoir, the sample holder section (which is surrounded by the Dewar chamber and the RF coil) and the last section goes through a home made photometer(Fig.6). Two optic fiver sensors enter the circuit to measure sample and water temperature. The circuit can be open or closed depending of the kind of experiment: for hydrating and loading the samples, a closed circuit is used. The water comes out of the reservoir pulled by the pump, goes through the sample holder, then trough the photometer and again to the reservoir . For the RF induced release experiments, the water ends in a second reservoir after passing the photometer.

2.3.1. Water circuit and pump: The water circuit is the core of the device. It must contain the sample in a fixed position since the RF field is generated only in a small region (see next section). At the same time must let the water to flow around the sample with a caudal small enough to let the gel reach the critical temperature when exposed to the RF field. It was necessary to construct a special sample holder with this purpose (Fig.7).

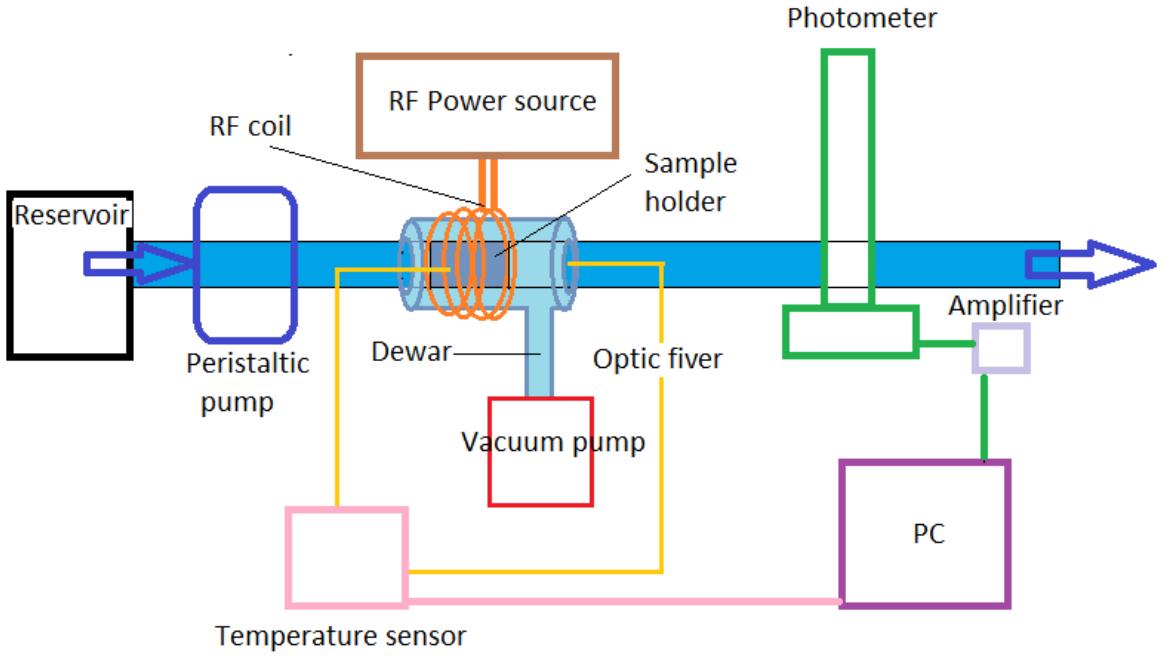

Figure 6. Complete device scheme.

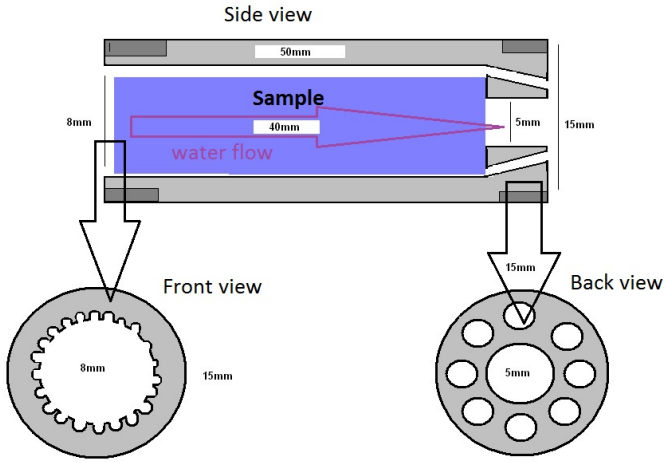

Figure 7. Design of the sample holder. Water enters the chamber from the left side and circulates around the sample through the small channels on the walls. The back wall has a smaller hole to stop the sample from moving with the flow.

- *Optimal caudal calculation*:
  The caudal of the water flowing through the circuit must be small enough to let the sample reach the transition temperature when the RF field is applied. If the caudal is too large, it will dissipate too much of the power generated by the sample and the temperature won't increase. So it's necessary to estimate the maximum

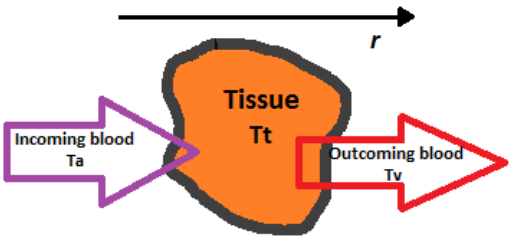

Figure 8. Penne's equation application scheme.A volume of tissue is irrigated by blood. Blood and tissue changes they temperatures by exchanging power

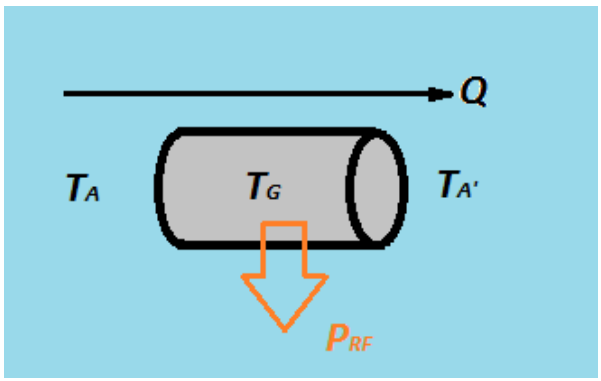

Figure 9. Penne's equation application scheme for the hydrogel in a water flow under a RF field.

caudal that can be used given the power dissipation characteristics of each sample. Using the Penne's bioheat equation

$$\rho_T c_T \frac{\partial T_T}{\partial t} = \frac{k_T}{r}\frac{\partial}{\partial r}[r\frac{\partial T_G}{\partial t}] + P_p + P_M \qquad \text{(III)}$$

with ρ_T, c_T, k_T and T_T the density, specific heat, thermal conductivity and temperature of the tissue respectively, P_M the metabolic power generated by the tissue and the perfusive power $P_p = \rho_S c_S Q \Delta T_{AV}$ with ρ_S and c_S the density and specific heat of the blood, Q the caudal and ΔT_{AV} the temperature difference between incoming and outcoming blood (Fig.8).

Applied to the hydrogel system in the simpler case of stationary and uniform T_T ($\frac{\partial T_T}{\partial t} = 0 = \frac{\partial T_T}{\partial r}$) taking $T_G = T_T$ as the gel's temperature and changing blood for water (Fig.9),it's possible to obtain an expression for the caudal in function of the power dissipation of the gel under RF field P_{RF} (instead of the metabolic power) and the desire temperature difference between incoming and outcoming water:

$$Q = \frac{P_{RF}}{\rho_A c_A \Delta T_{AA'}} \qquad \text{(IV)}$$

Using the results of the calorimetric measurements of the samples under RF field in IV,the maximum caudal was obtained for a water temperature difference of 1K.

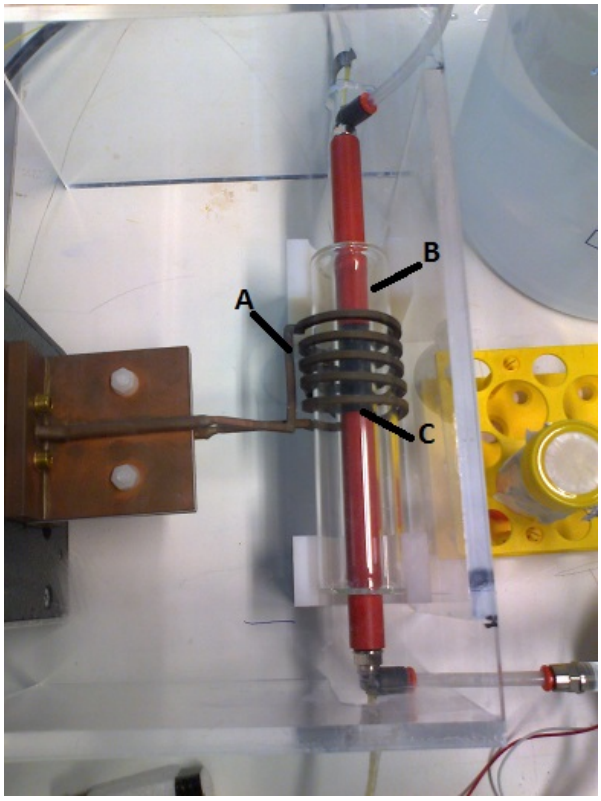

Figure 10. Top view of a section of the device. A=RF coil, B=Dewar, C=Sample holder

With this information, a peristaltic pump was built from a OEM component(Watson Marlow 400F/D3).

2.3.2. RF field generator : The excitation RF field is generated by the same equipment used for the power dissipation measurements of the samples. The water circuit goes through the coil of the applicator so the sample holder occupies the maximum field region(Fig.10).

2.3.3. Dewar : Since the coil of the RF generator is circulating big currents ($\sim 600A$), its working temperature is high ($\sim 80^oC$) even with the chiller circuit on. This fact makes necessary to isolate the water circuit from the thermal contact with the coil with a Dewar like vacuum chamber (Fig.10). The glass chamber surrounds the sample holder and is connected to a turbomolecular pump which maintains the pressure inside the chamber around 10^{-7}mbar (Fig.11).

2.3.4. Photometer : In order to have a real time reading of the B12 concentration in the water flow, a home made photometer was built and added to the last part of the circuit (Fig.12). It consists of a couple of photodiodes (Centronic BPW21) with a 600nm lowpass interference filter (Edmund Optics) placed under the water tube. The

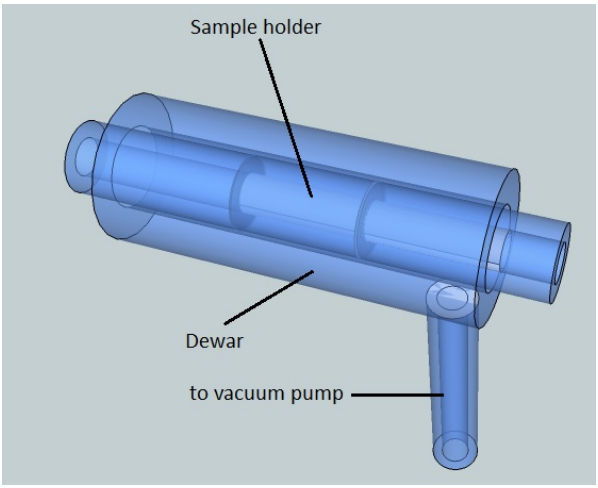

Figure 11. Section of the circuit. Sample holder inside vacuum chamber

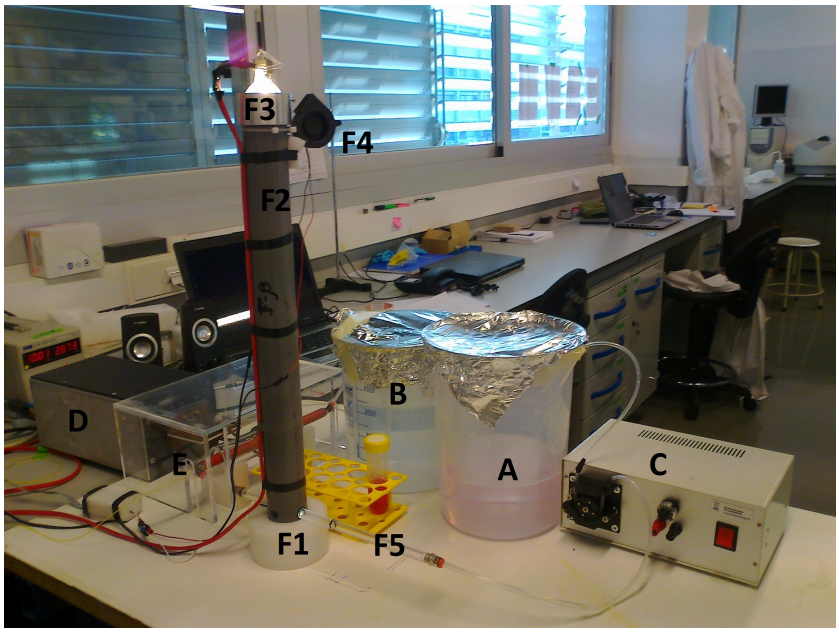

Figure 12. Picture of the device in open circuit configuration. MiliQ water comes out of the recipient **B** pulled by the pump **C**, goes through the sample holder **E** inserted in the RF field coil **D**, then pass trough the photometer ending in the recipient **A**. The photometer consist in a base **F1** which contains to photodiodes under a optic filter (not shown in the picture). The light from the lamp **F3** is guided by the reflective inner surface of the tube **F2** and goes through the circulating B12 solution **F5** before reach the diodes. The blower **F4** helps to dissipate the heat generated in the lamp.

signal of the diodes is amplified and digitalized so it can be seen in real time as a voltage vs. time plot in a computer. A commercial halogen lamp is used as light source. The optic filter and diodes were selected so the device is sensitive to the variations in light intensity in the range [450-600]nm which contains the visible absorbance maximum of B12 vitamin (Fig.13).

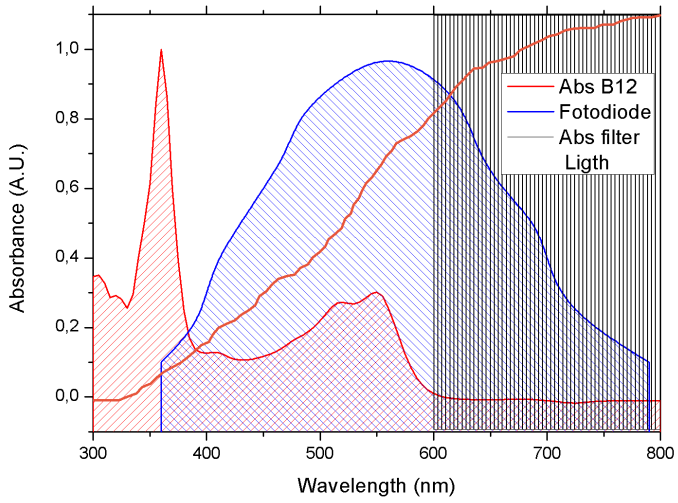

Figure 13. Absorption spectra of the vitamin B12 (red) togehter with sensibility of the diodes (blue), absorbance of the filter (black) and emittance of the light source (orange).

- Photometer calibration: To be able to obtain absolute concentration measurements from the photometer and determinate the sensibility range, a calibration protocol was designed: the device started reading when only MiliQ water was flowing through the closed circuit. Small volumes of a concentrated B12 solution were added to the circuit reservoir at known intervals letting the reading to stabilise. From the average value of each plateau and the corresponding calculated concentration, a calibration curve diode voltage vs. concentration was carried out.

2.4. Release experiments

2.4.1. Blank : A dry sample of hydrogel without MNP (blank) was first hydrated in MiliQ water by putting it in the sample holder and circulating the water for 24h. Then, the photometer was started, and 15mg of solid B12 was added to the circuit reservoir containing 17,5 ml of MiliQ water. Finally, the reservoir was changed for another one containing clean MiliQ water and the circuit was open so, after flowing through the photometer, the water leaved the system. In this stage the RF field was turned on for 5 minutes.

2.4.2. Ferrogel : A dry sample of ferrogel was introduced inside the device and rehydrated by circulating a solution of B12 (1.034(5)g/l) for 24h in closed configuration. Then, the solution was replaced by pure MiliQ water and circulated for 2h with the circuit in open configuration to wash the less attached vitamin. After that time, with the MiliQ water still in circulation, the field was turned on for 66s. The field application was repeated 80 minutes later and a third time 75 minutes after the second.

3. Results

3.1. Sample characterization

3.1.1. VSM : Figure 14 shows the results for the magnetization measurements of ferrogel and blank. The blank response is a diamagnetic curve with a slope of -3.52$\frac{Am^2}{Tkg}$ which is typical for organic materials like the components of the hydrogel. The ferrogel response is clearly SPM with a saturation magnetization of 13.23(1)$\frac{Am^2}{Tkg}$ and negligible remanence of 0.10(1)$\frac{Am^2}{Tkg}$ and coercive field of 1.3(1)G.

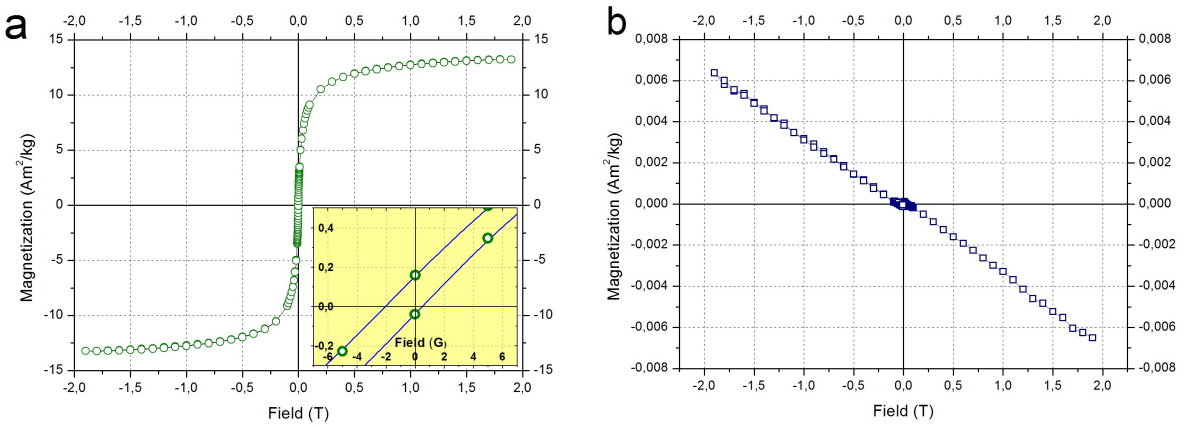

Figure 14. Magnetization(magnetic moment per sample mass) vs. field plot for ferrogel(a) and blank(b). The response of the blank is clearly diamagnetic. The ferrogel curve corresponds to a practically SPM response with very small remanence and coercive field(magnification inserted). Offset due off-centered sample.

3.1.2. SEM : Figures 15, 16 and 17 show the topology of the gels. Besides of the expected pore structure([20,100]μm pore size),small clusters of micron size can be seen in all images of blank and ferrogel samples. The amount of clusters tend to increase when temperature rises and humidity decrease. Although the measurements were made in low vacuum conditions ([540, 760]Pa), the initially hydrated samples lose all its water in the process ending the experiment completely dried. Changes in the structure of the pores can be notice between the beginning and the end of the measurements.

3.1.3. TEM : From the conventional TEM result shown in figure 18, a MNP average size of approximately 10nm can be observed. The MNP appear agglomerated in clusters inside the gel.

The measurements of the vitrificated samples was difficult. The quantity of material attached to the grid was very little and, even at liquid nitrogen temperature, the electron beam deteriorates the sample which reacts with violent movements preventing to take long exposition images. Even so, a net structure three orders of magnitude smaller that the one observed by SEM can be notice in Fig. 19.

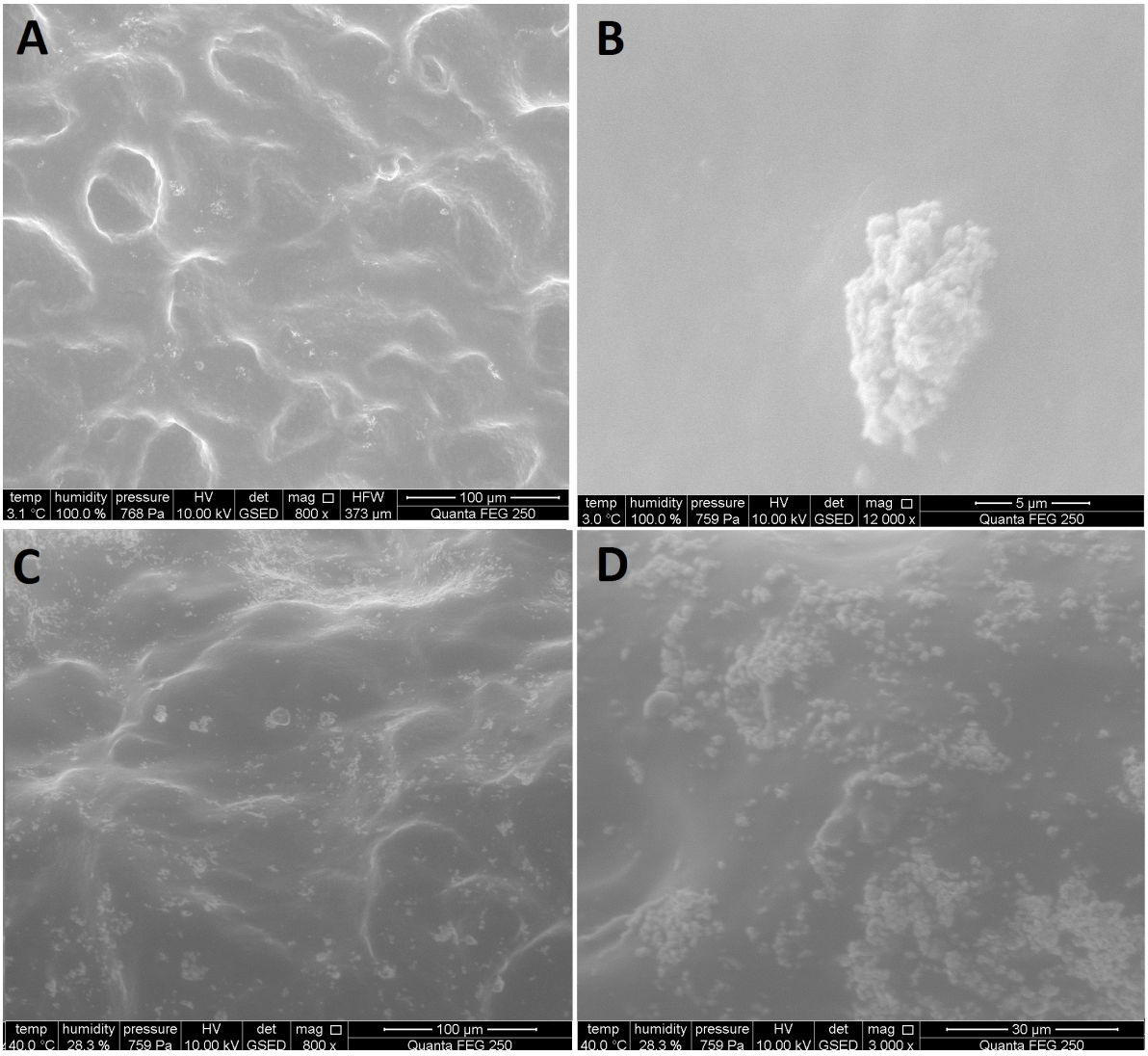

Figure 15. SEM images from the blank sample taken at 760Pa where the pore structure of the gel can be notice. At low temperature and high humidity (**A**, **B**) small clusters can be seen. At high temperature and low humidity (**C**, **D**)the number of cluster increase.

Trying to obtain an image of the MNP inside the gel, the EDS analysis was performed in all the available material in the grid(Fig. 20). Although the presence of Fe was confirmed, no MNP could be observed. Instead, multiple materials contamination was detected in form of micro and nanoparticles like the one shown in figure 20.

3.1.4. RF response : Figure 2 shows a representative temperature vs. time measurement of a sample of ferrogel while exposed to the RF field. After a short transition time, the curve turns linear so the process can be taken as adiabatic. A linear function fit of the adiabatic section of the curve was used to obtain the slope $\frac{\partial T}{\partial t}(0)$ for the power dissipation calculation II. The final value of 1.73(1)W for a field amplitude of 45kA/m was the result of a three determinations average. With this information, a

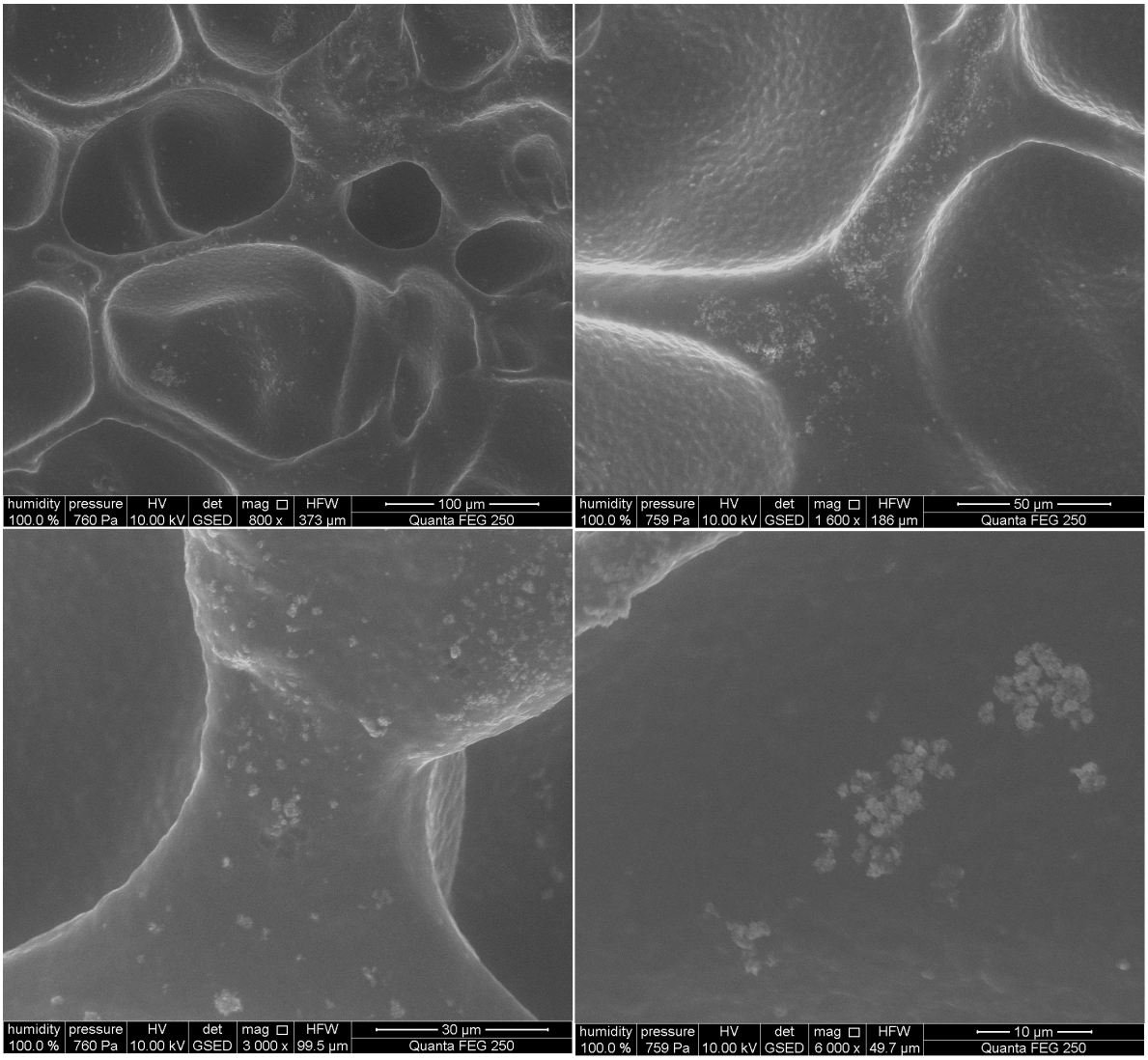

Figure 16. SEM images from the ferrogel taken at 760Pa, 3^{o}C and 100% RH. Cluster structures similar to those in the blank appear.

maximum caudal of 0.41ml/s was calculated to maintain a 1K difference between the extremes of the sample.

3.2. Photometer calibration

From the voltage vs. time curve obtained directly from the diodes (Fig.21) a calibration curve was made (Fig. 22) which shows a typical Lambert-Beer exponential dependence between the diode voltage and the B12 concentration in the water flow:

$$V(c) = Ae^{-c/\tau} + V_0 \qquad \text{(V)}$$

Where c is the concentration, $A+V_0$ is the value of the signal whit pure MiliQ water circulating ($c = 0$) and τ is the constant where the optic path and the molar extinction coefficient are contained. While the value $A + V_0$ depends on the light intensity emitted

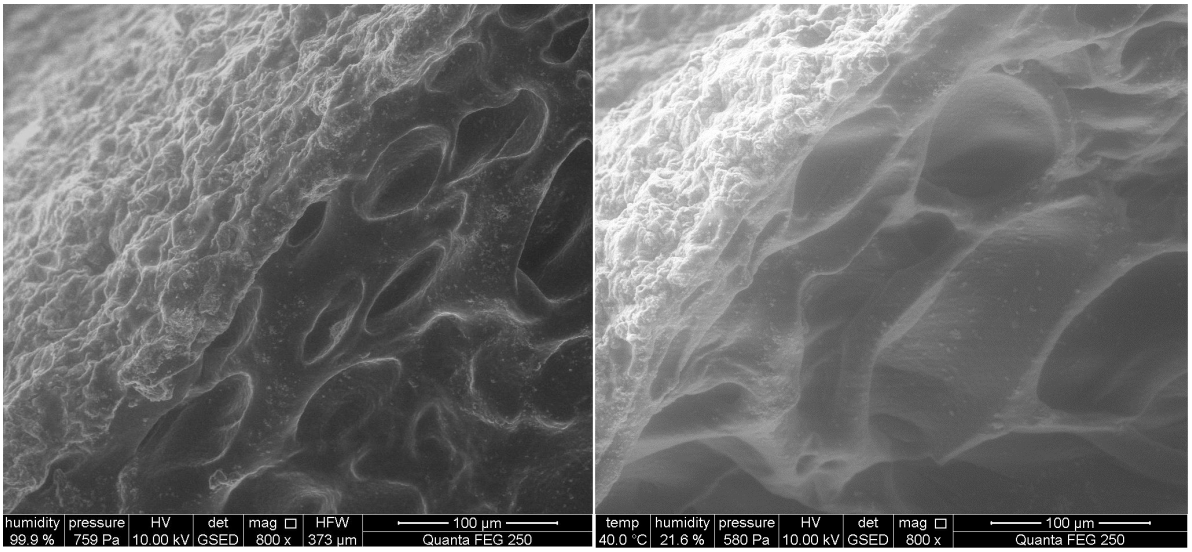

Figure 17. SEM images from the same section of a ferrogel sample in the initial measurement conditions: 3^oC, 760Pa, 100%RH (left) and final measurement conditions: 40^oC, 580Pa, 21.6%RH(right). Differentiated surface and lateral section can be observed. Structural modifications can be notice.

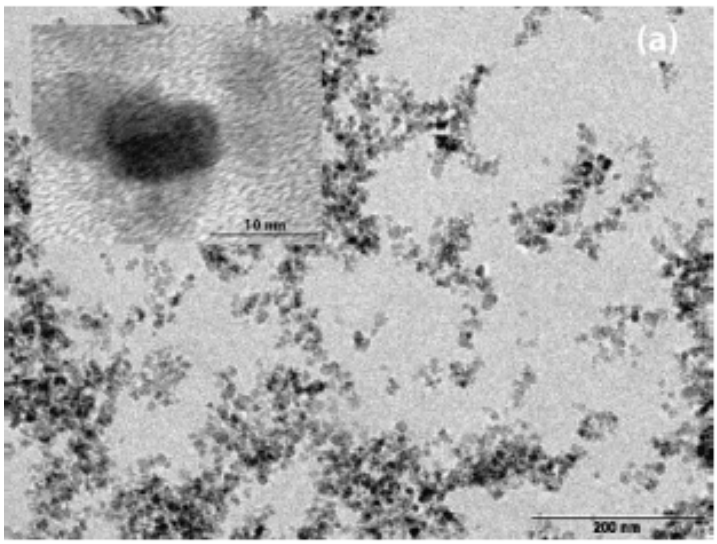

Figure 18. Representative TEM images of the MNP inside the gel. The particles appear agglomerated with a individual average size of 10nm (image from [13]).

by the lamp, τ must be the same for all the calibrations if the absorbent substance and the geometry of the photometer remains unaltered.
The exponential fit confirms the linear relation between the light intensity and the diodes signal since the later maintain the same Lambert-Beer dependence with the concentration than the first should follow in the conditions of the experiment [16].

Six closed tubes filled with B12 solutions at different concentrations were assembled to perform periodic calibrations. The tubes have exactly the same geometry and

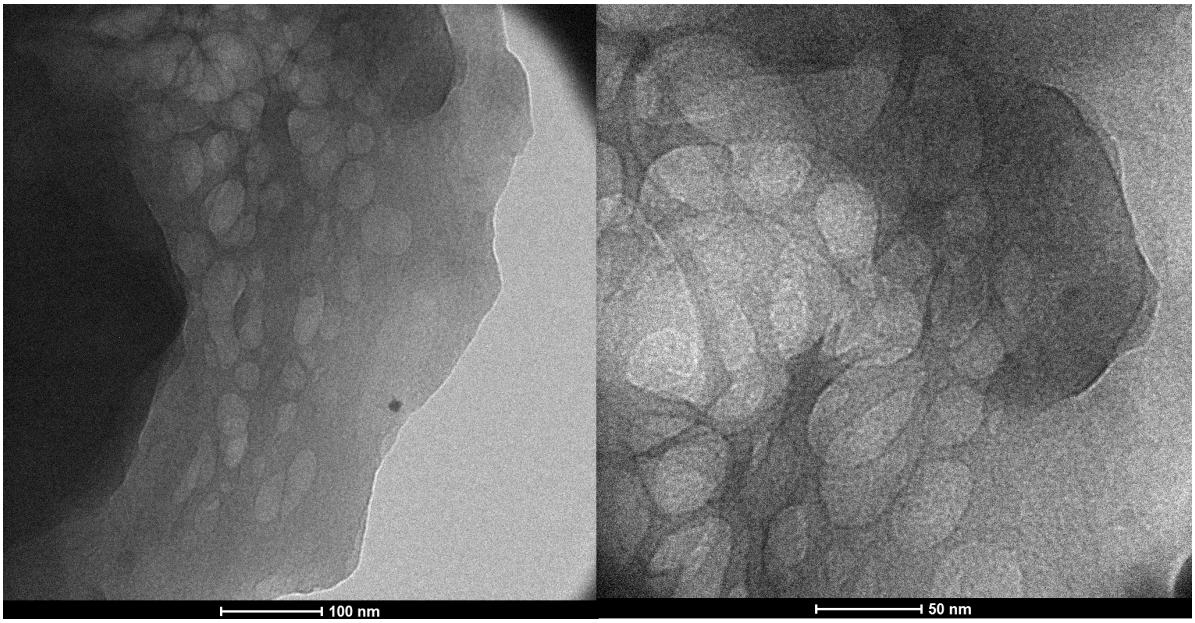

Figure 19. TEM images of the vitrificated ferrogel sample. A net structure with 50nm holes can be noticed.

constitution of the one in the photometer and can be exchanged with these one. This system allows to perform the calibration protocol in less than 10 minutes.

3.3. Release experiments

3.3.1. Blank : The voltage readings from the diodes in function of time for the three stages of the experiment show the response of the photometer to the change in light intensity due the variations in B12 concentration. The system was able to detect even the bubbles circulating trough the circuit (Fig.23). No effect of the field exposure was detected.

3.3.2. Ferrogel : Figure 24 shows the data from the field induce liberation experiment described in 2.4.2. In **A**, the complete record is shown: the initial signal of 2V corresponds to the circulating B12 solution used to load the gel for 24h (time scale was restarted). Around t=20mn the B12 is replaced by pure MiliQ water to wash the whole device and the sample so the only B12 left is that inside the gel. After 100mn the signal was stable in the c=0 equivalent value. Magnification of the three liberation events induced by the field application are shown in **B**, **C** and **D**. The correlation between liberation and field application is clear since the effect of the field can be seen in the data as electromagnetic noise before every concentration peak. The amount of vitamin released by the gel is smaller each time.
From the acquired data is possible to determine the absolute mass m of B12 vitamin expelled each time. Converting the voltage values $V(t)$ to concentration $c(t)$ by the equation V, the amount of B12 liberated is equal to the peak area ,which can be

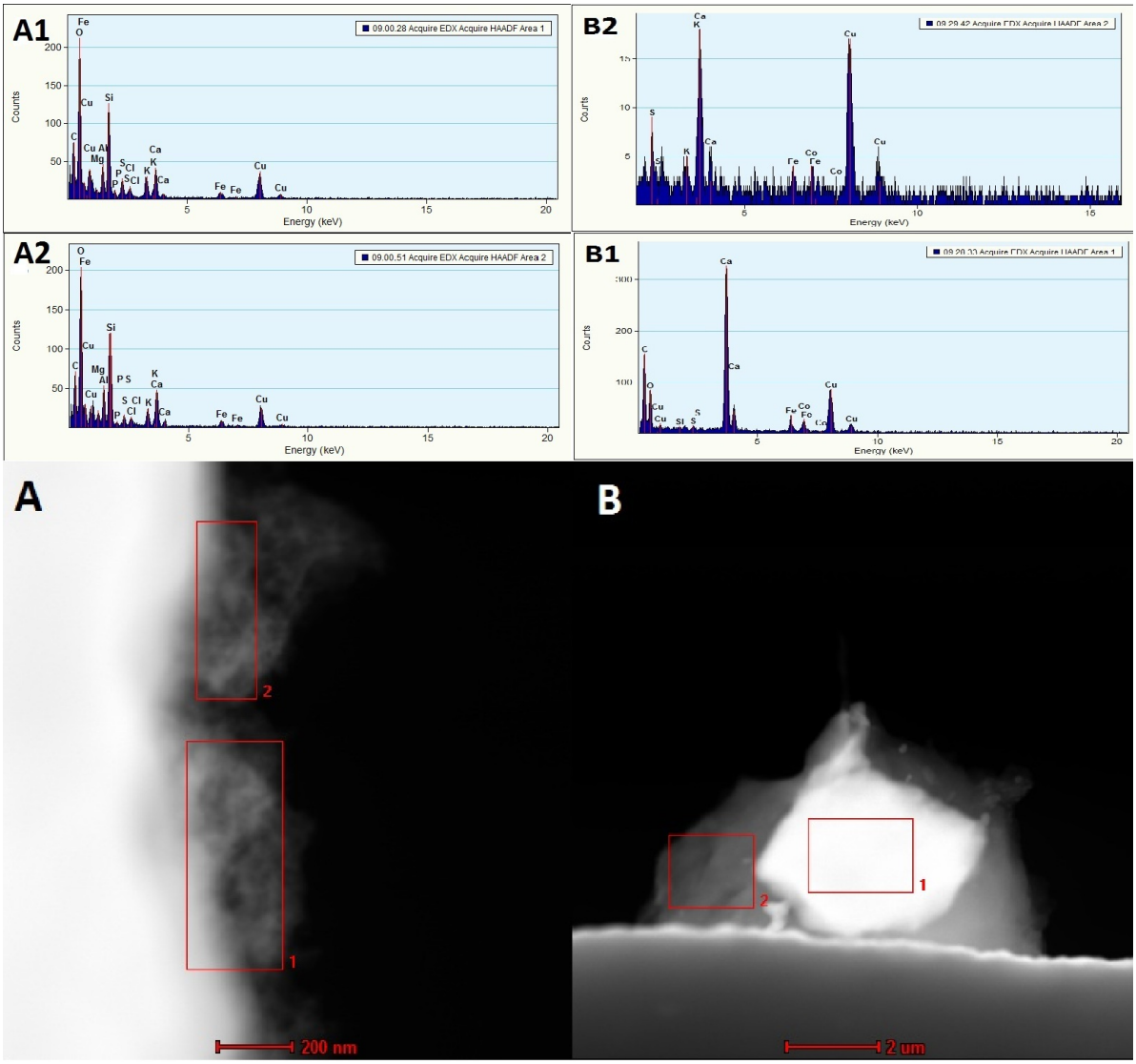

Figure 20. STEM images an EDS analysis of the ferrogel sample. Small peaks correspondig to Fe presence can be notice but no MNP was could be detected. A micron size particle of Ca is shown in B has example of the contamination.

estimated by a numerical integration, multiplied by the caudal Q :

$$m = Q \int_{t_0}^{t_f} c(t)\, dt \tag{VI}$$

where t_0 and t_f determine the duration of the liberation event. Using VI with the first peak, a liberated B12 mass of 25.3(2.6)ng is obtained.

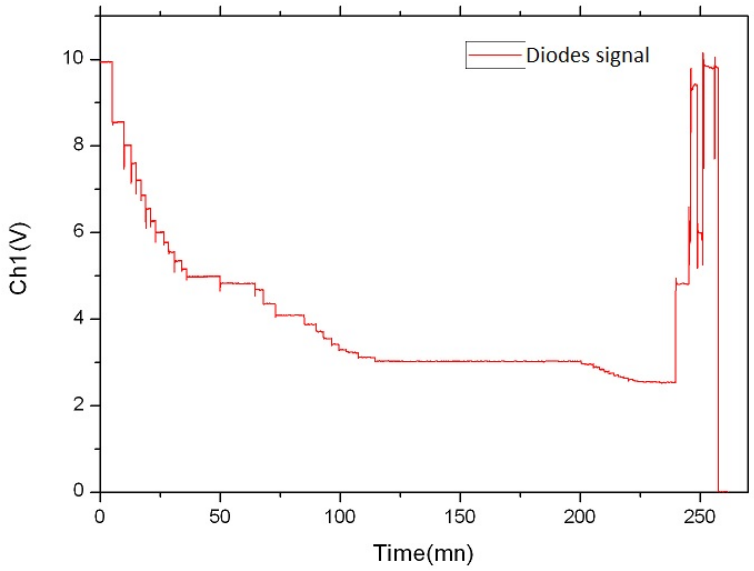

Figure 21. Voltage vs. time plot of the calibration experiment. Starting with pure water (maximum signal), small volumes of concentrated B12 solution were added every certain time. Each addition rises the B12 concentration in the circuit provoking a decrease in the light intensity reaching the diodes and therefore, a decrease in the signal.

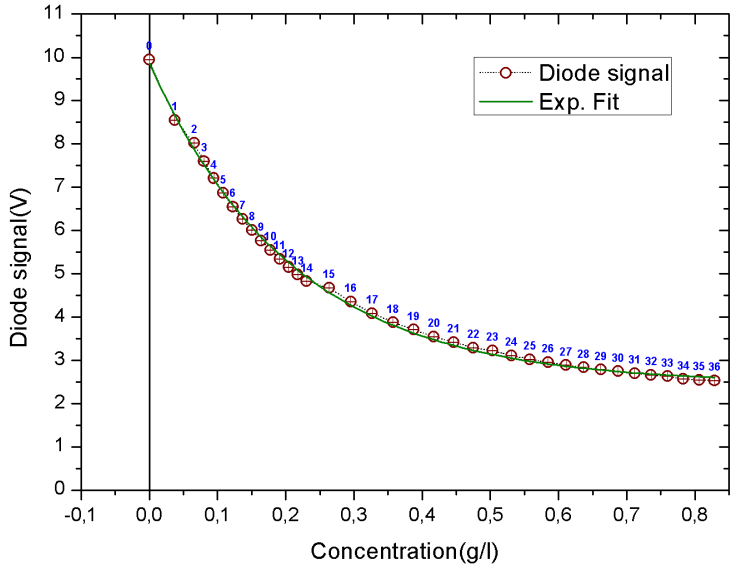

Figure 22. Voltage vs.concentration plot from the calibration experiment. The voltage is proportional to the light intensity in the range [450-600]nm. The average values from every plateau in the voltage vs. time plot were plotted vs. the calculated concentration. A typical Lambert-Beer exponential dependence can be notice.

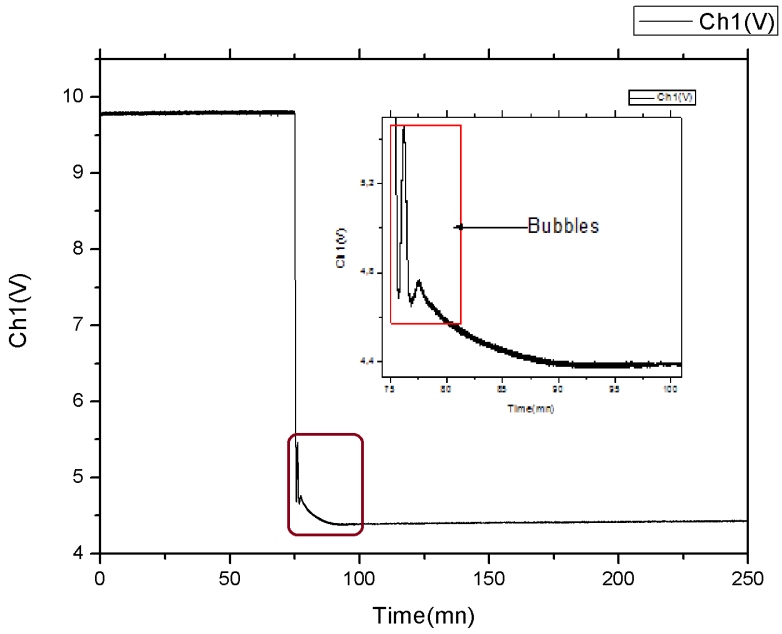

Figure 23. Diode voltage vs. time plot corresponding to the first experiment where B12 vitamin is added to the circulating water. A very significant drop in the light intensity can be seen when the diluted B12 reaches the photometer (t∼75mn). The signal stays steady when the B12 is equally distributed in the whole circuit.Insert: Magnification of the red square. Light intensity fluctuations caused by air bubbles in the circuit

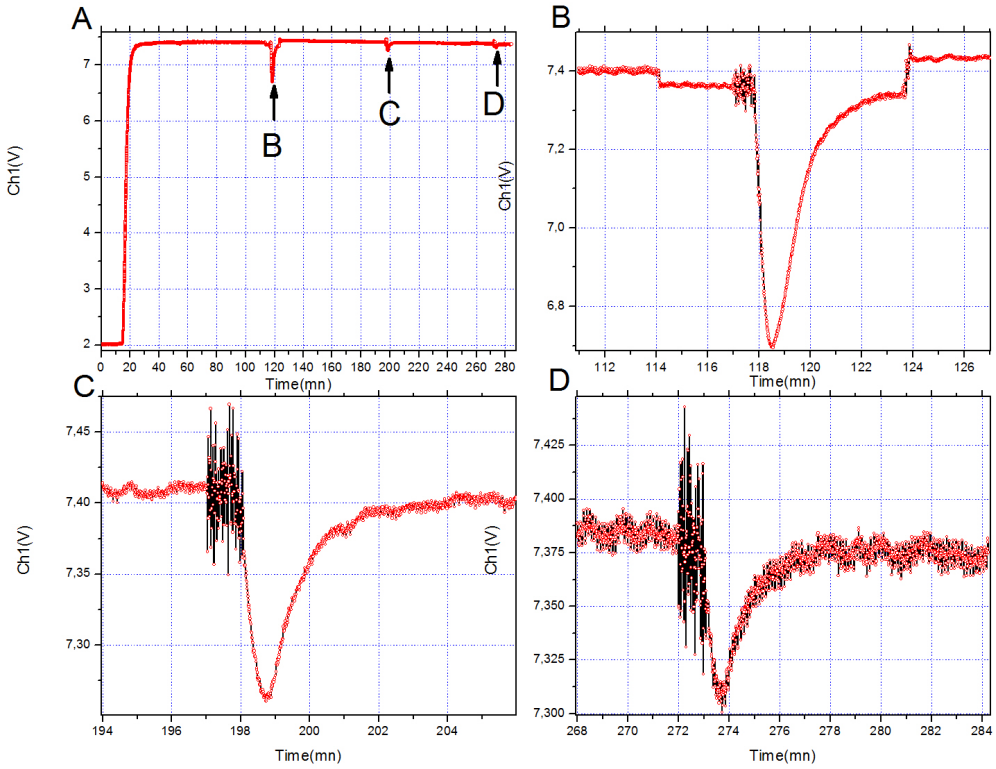

Figure 24. Results of the field induced liberation experiment with the ferrogel. The Y axis voltage (Ch1) is proportional to the light intensity reaching the diodes and so, it can be translated to B12 concentration through expression [16]. **A** shows the complete experiment: the initial signal of 2V corresponds to the B12 solution circulating. Then, around t=20mn, the solution is replaced by pure MiliQ water and the signal rise to 7.4V. In t={120mn, 200mn, 274mn} the peaks of concentration produced by the field induced liberation can be seen. Magnifications of the peaks shown in **B**, **C** and **D**. The interference before every peak is caused by the RF field.

4. Discussion and conclusions

The are two aspects to speak about in this work: the sample characterization and the device design, construction and performance. Although the original motivation was only the first, problems with the RF generator prevented from continuing with the experiments and achieve a complete characterization of the drug release process. Also, the design, construction and calibration of the device proved to be a complex and interesting objective on his own.

4.1. Sample characterization

The morphology of the gel was studied by low vacuum SEM and cryo-TEM. Since the conventional TEM measurements were done by the collaboration that synthesized the samples, the intention was to exploit INAs facilities and study the gels in his native state i.e. hydrated. This proved to be very difficult due to the extreme sensibility of the samples to the environmental conditions.
The aim of the environmental SEM experiment was to try to observe the structural face transition of the sample. Although this device is designed to perform the measurements in a more "biological samples friendly" conditions than the conventional SEM, it wasn't enough for the hydrogels. The 760Pa pressure is still much smaller than the atmospheric value and the initially hydrated gel lose his water content very fast. However, the general pore structure of the gel was observed with good definition at the micron scale. Also, a difference between the aspect of the sample at 3^oC and 40^oC was observed. The ferrogel sample was study first so the micron sized clusters were expected to be made of MNP, but the posterior observation of the same objects in the blank sample eliminate that possibility. This finding indicates that the cluster are made of the same material of the gel. The irreversible proliferation of the clusters with the temperature rising suggests that they are the product of some kind of degradation process in the material.
The cryo-TEM measurements were less productive. In the same direction of preserving the native structure of the sample, the conventional fixation process for soft specimens was avoided. The sample reacted not so well to the vitrification process and a very small quantity ended in the copper observation grid. Also, as already stated in 3.1.3, the electron beam provoked the small pieces of gel to jump out of the grid. With these conditions it was impossible to obtain even one image of a MNP.
The STEM-EDS measurements were able to confirm the existence of Fe in the sample (although this was already evident from the magnetization and calorimetric experiments commented ahead) but also failed to provide a MNP visualization. Instead, a lot of particles of a priori unexpected compositions appeared. This contamination couldn't be explained yet.
The principal conclusion from this results is that a better technique to preserve the native state of the sample during TEM observation must be found.
The magnetic and power dissipation responses of the samples were the expected one: a clearly SPM response typical for magnetite MNP of that size in the ferrogel, and

a regular biomaterial diamagnetism in the hydrogel without particles. This correlate perfectly with the existence of power dissipation only for the ferrogel under a RF field.

4.2. Device performance

The preliminary results shown in 3.3.2 could be considered as a solid success of the device. Although the optimal measurement conditions must be found yet, it seems that the system is robust enough to perform a wide variety of experiments with trustful results.
The possibility of varying field strength, caudal and photometer sensibility, the system can be used to characterise a wide variety of samples in very different conditions. The strongest limitation with the current design is in the test drug to be used, since the maximum sensibility of the photometer is fixed in the visible absorption peak of B12 vitamin. This limitation can be solved constructing a set of several interchangeable diode and filter pairs. Three should be enough to cover most of the UV-Vis spectrum. The temperature sensing capability of the device wasn't tested yet because of the problem with the RF generator. A simultaneous concentration and water/sample temperature reading will be a significant improvement in the system.

5. Acknowledgements (in Spanish)

A Gerardo, mi director. Por darme esta oportunidad, por la paciencia que me tuvo y por la que no me tuvo también.
A Rebeca Hernández y Carmen Mijangos por proveerme de las muestras.
Al personal del LMA: Carlos, Teo, Alfonso, Laura y en especial a Rodrigo Fernández-Pacheco, que hizo de mis muestras su ballena blanca.
Al personal del taller del INA. En especial a Luis Tejero, en cuyo torno se gestó gran parte del monstruo.
Al Servicio de Instrumentacin Electrónica de facultad de ciencias de la UNIZAR.
A mis amigos, nucleados mayoritariamente en el ComIDA tupper group. Sin esas sobremesas hubiera terminado un poco antes pero me hubiera divertido muchísimo menos.
A esa ayuda muy especial en la intensa recta final, que entre muchas otras cosas me contuvo, me retó para que trabajara y luchó contra mi chapusera angloverborragia .
Al *ingenieri desarmista* Pablo Mereles por su aporte al aparato, que felizmente cumple su función de evitar (nuevos) incendios.
Al Dr. Daniel Schinca del Centro de Investigaciones Ópticas (CIOp-Argentina) por la inspiración previa y la asistencia posterior con el fotómetro.
A los docentes del máster que, además de soportarme en las clases, toleraron mi rodeo migratorio.

6. References

[1] Pankhurst, Q.A. et al. "Progress in applications of magnetic nanoparticles in biomedicine." Journal of Physics D: Applied Physics 42 (2009): 224001

[2] Q A Pankhurst et al 2003 J. Phys. D: Appl. Phys. 36 R167

[3] Jordan, A.; Scholz, R.; Wust, P.; Fhling, H.; Felix, R. Magnetic fluid hyperthermia (MFH): Cancer treatment with AC magnetic field induced excitation of biocompatible superparamagnetic nanoparticles. J Magn Magn Mater 1999, 201, 413419.

[4] Satarkar, Nitin S, and J Zach Hilt. "Magnetic hydrogel nanocomposites for remote controlled pulsatile drug release." Journal of Controlled Release 130.3 (2008): 246-251.

[5] Albert Figuerola, Riccardo Di Corato, Liberato Manna, Teresa Pellegrino, From iron oxide nanoparticles towards advanced iron-based inorganic materials designed for biomedical applications, Pharmacological Research, Volume 62, Issue 2, August 2010, Pages 126-143, ISSN 1043-6618, 10.1016/j.phrs.2009.12.012.

[6] Tartaj, P.; Del Puerto Morales, M.; VeintemillasVerdaguer, S.; Gonzalez-Carreo, T.; Serna, C.J. The preparation of magnetic nanoparticles for applications in biomedicine. J Phys D: Appl Phys 2003, 36, R182 97.

[7] Gazeau, F.; Levy, M.; Wilhelm, C. Optimizing magnetic nanoparticle design for nanothermotherapy. NanomedicineUK 2008, 3, 831844.

[8] O. Wichterle, D. Lim, Nature 1960, 185, 117; [1b] N. A. Peppas, A. G. Mikos, Hydrogels in Medicine and Pharmacy, CRC Press, Boca Raton, FL 1986, p. 1

[9] T. Tanaka, Phys. Rev. Lett. 1978, 40, 820; [2b] T. Tanaka, I. Nishio, S. T. Sun, S. Ueno-Nishio, Science 1982, 218, 467

[10] Echeverria, Coro, and Carmen Mijangos. "UCST-Like Hybrid PAAm-AA/Fe3O4 Microgels. Effect of Fe3O4 Nanoparticles on Morphology, Thermosensitivity and Elasticity." Langmuir (2011).

[11] Hernández, R.; Mijangos, C. Macromol. Rapid Commun. 2009, 30, 176.

[12] Hernández, R.; Sacristan, J.; Nogales, A.; Ezquerra, T. A.; Mijangos, C. Langmuir 2009, 25, 13212.

[13] R. Hernández, J. Sacristán, L. Asín, T. E. Torres, M. R. Ibarra, G. F. Goya, and C. Mijangos J. Phys. Chem. B, 2010, 114 (37), pp 1200212007

[14] R. Hernández, Mijangos, C.. Private communication.

[15] Hernández, R.; Zamora-Mora, V.; Sibaja-Ballestero, M.; Vega Baudrit, J.; López, D.; Mijangos, C. J. Colloid Interface Sci. 2009, 339,53.

[16] J.H. Lambert, Photometria sive de mensura et gradibus luminis, colorum et umbrae [Photometry, or, On the measure and gradations of light, colors, and shade] (Augsburg ("Augusta Vindelicorum"), Germany: Eberhardt Klett, 1760). p. 391

[17] Fernandez Pacheco R. (LMA-INA).Private communication